INTERNATIONAL DENTAL JOURNAL 000 (2024) 1–15

Unravelling the Programmed Inflammation and Tissue Repair by a Multipotential Antimicrobial K21 Silane

Umer Daood [a,l*], *Muhammad Sharjeel Ilyas* [b], *Sehar Bashir* [c], *Neelofar Yousuf* [d], *Maryam Rashid* [d], *Kanwardeep Kaur* [e], *Ranjeet Ajit Bapat* [a], *Mohammed Nadeem Bijle* [f], *Malikarjuna Rao Pichika* [g], *Kit-Kay Mak* [g], *Shiming Zhang* [h], *Zeeshan Sheikh* [i], *Abdul Samad Khan* [j], *Ove Peters* [k,l], *Jukka P Matinlinna* [m,n]

[a] *Restorative Dentistry Division, School of Dentistry, International Medical University Kuala Lumpur, Kuala Lumpur, Malaysia*
[b] *Oral Biology, Akhtar Saeed Medical and Dental College, Lahore, Pakistan*
[c] *Histopathology, Akhtar Saeed Medical and Dental College, Lahore, Pakistan*
[d] *Pharmacology, Akhtar Saeed Medical and Dental College, Lahore, Pakistan*
[e] *Clinical Oral Health Sciences Division, School of Dentistry, International Medical University, Kuala Lumpur, Malaysia*
[f] *Paediatric Dentistry, Faculty of Dentistry, The University of Hong Kong, Hong Kong SAR, China*
[g] *School of Pharmacy, International Medical University Kuala Lumpur, Kuala Lumpur, Malaysia*
[h] *Interdisciplinary Institute of Life Medicine, Hunan University, Changsha, Hunan Province, China*
[i] *Biomaterials & Applied Oral Sciences (BAOS), Dental Clinical Sciences, Faculty of Dentistry, Dalhousie University, Halifax, Nova Scotia, Canada*
[j] *Department of Restorative Dental Sciences, College of Dentistry, Imam Abdulrahman Bin Faisal University; Dammam, Saudi Arabia*
[k] *Department of Endodontics, Arthur A Dugoni School of Dentistry, University of the Pacific, San Francisco, California, USA*
[l] *School of Dentistry, The University of Queensland, Herston, Queensland, Australia*
[m] *Dental Materials Science, Applied Oral Sciences & Community Dental Care, Faculty of Dentistry, The University of Hong Kong, Hong Kong SAR, China*
[n] *Biomaterials Science, Division of Dentistry, School of Medical Sciences, The University of Manchester, Manchester, UK*

ARTICLE INFO

Article history:
Received 14 July 2024
Received in revised form
4 September 2024
Accepted 6 September 2024
Available online xxx

Key words:
Laser Raman
Macrophage, Polarisation
M1
M2
Cytotoxicity
Burn

ABSTRACT

Aims and Objectives: To examine if a novel antimicrobial silane K21 can alter macrophage polarisation and affect fibroblast proliferation by deciphering the molecular pathways for programmed healing using a combined *in vitro* and *in vivo* (animal) burn model.
Materials and Methods: An injectable silane-based antimicrobial aimed to modulate macrophage polarisation was manufactured. Experimental analysis included colorimetric cell migration assays on gingival fibroblasts, macrophage phagocytosis characterisation, immunofluorescence staining, triacylglycerol accumulation within macrophages by LCMS, cellular metabolic/proliferation assays, macrophage exposure quantification with morphology assessment using FE-SEM, Raman spectral analysis, RNA isolation for relative gene expression and animal study model to morphometrically and microscopically analyse partial thickness burn wound healing under QAS/K21.
Results: M1 and M2 polarisation both appeared exaggerated under QAS/K21 treatment. The wounds treated with K21 had depicted accelerated healing as compared to control ($P < .05$) in dorsal skin of rabbits. Relative gene expression results demonstrate reduced cytokine and anti-inflammatory response under the influence of K21. While M1 expression, TG

* Corresponding author. Restorative Dentistry Division, School of Dentistry, International Medical University Kuala Lumpur, 126, Jalan Jalil Perkasa 19, Bukit Jalil, 57000 Bukit Jalil, Wilayah Persekutuan, Kuala Lumpur, Malaysia.
E-mail address: umerdaood@imu.edu.my (U. Daood).
Umer Daood: http://orcid.org/0000-0002-7631-1628
Muhammad Sharjeel Ilyas: http://orcid.org/0000-0002-5552-0236
Mohammed Nadeem Bijle: http://orcid.org/0000-0002-7205-9891
https://doi.org/10.1016/j.identj.2024.09.012

accumulation, and associated characterisations demonstrate the programmed inflammatory potential of K21.

Conclusion: the antimicrobial and reparative efficacy of K21 silane aids in programmed inflammation for enhanced tissue healing and repair.

Introduction

Biomaterials, when introduced inside biological bodies, induce immune responses with macrophages getting polarised into various subsets that influence the biological behaviour of cells.[1] The environmental signals determine macrophage polarisation in different directions, leading to pro and anti-inflammatory subtypes. Therefore, in frontline research, the polarisation of macrophages has become an important and most sought topic.[2] Previous studies have shown M1 macrophage polarisation, required for early repair, may get inhibited if the process persists for longer term.[3] There is a release of several anti-inflammatory factors which include IL10, IL4 and TGF-β that promote differentiation of precursor cells.[4] This is the remarkable phenotypic plasticity conveniently describing a continuum of macrophage phenotypes due to its polar values.[5,6] In this paper, we focus on the ways of biochemically induced M1 and M2 polarisation of macrophages against a known antimicrobial biomaterial for the purpose of wound repair and healing.

Quaternary ammonium salts are a type of positively charged surfactants[7] that exhibit electrokinetic effects at the boundary between a solid and liquid. This effect occurs due to the existence of hydrophilic and lipophilic groups inside the surfactant molecules. These compounds have a higher concentration of electric charge inversion, which effectively works as a potent antibacterial agent against micro colonies of bacteria with negatively charged surfaces. This indicates that they possess a very potent capacity to penetrate (Figure 1) because of their high electric charge inversion, which suppresses the van der Waals forces (electrostatic shielding effect) of the cell.[4] The hydrocarbon tail of the cationic amphiphilic substance inserts into the hydrophobic interior of the cell membrane, resulting in charged interactions. Despite the presence of hydrophobicity resulting from quaternisation, the molecule exhibits enhanced water solubility. The surfactant feature of this substance enables the creation of a protective layer on a surface, resulting in the production of an antimicrobial film and aiding in the prevention of biofilm formation.[8]

Raman spectroscopy is a sensitive and essential method for analysing biological material. It is non-invasive and requires minimum sample preparation.[9,10] Raman spectroscopy is less susceptible to interference from water absorption compared to other spectroscopic techniques,[11] enabling more accurate observations at greater depths. Additionally, it has the capability to determine functional polarisation of macrophages. This study aimed to assess the efficacy of combining Raman spectroscopy with multivariate statistical analysis, namely principal component analysis (PCA), in reliably distinguishing between M1 and M2 macrophage phenotypes in vitro. The objective of the study was to investigate if K21 can alter macrophage polarisation and affect fibroblast proliferation by deciphering the molecular pathways for programmed healing using a combined *in vitro* and *in vivo* (animal) burn model. The null hypothesis examined was that K21 solution would not alter macrophage polarisation and promote the healing of burn wounds. In addition, K21 solution will not affect the fibroblast proliferation hence assisting in the treatment of inflammation.

Materials and methods

Development of quaternary ammonium solution (QAS)

In this *in vitro* and *in vivo* laboratory research, we developed an injectable silane-based[12] antimicrobial with antibacterial characteristics (Figure 1-Supplemental Figure 1**).** This investigation used a novel antibacterial substance called Quaternary Ammonium Silane (QAS; KHG FiteBac Technology, Marietta, GA, USA). QAS/K21 has a functional terminal-OH group that can initiate reactions with other -OH groups.[13]

The sol gel method was used to make the QAS (K21) silane solution. This was done by properly diluting the K21 (QAS (k21); KHG FiteBac Technology, Marietta, GA, USA) organosilane in 100% absolute ethanol. The target pH was within the acidic range (5-6.5). The QAS/K21 solution was diluted with ethanol to create test solutions with ***concentrations of 0.46% and 1% of QAS/K21***. These were then utilised to carry out several stages of research trials. Following the determination of the outcomes for the K21 solution at a concentration of 0.46%, the animal models were then subjected to a single concentration.

In-vitro cell migration test of K21 in human primary gingival fibroblasts cells

Human primary gingival fibroblasts (PGF) were isolated from the jaw of a 65-year-old Caucasian male obtained from ATCC (HGF, PCS-201–018, ATCC, USA).

Media and culture conditions

To initiate an experiment, a working frozen culture was thawed at approximately 37°C and grown in tissue culture flasks with fibroblast basal medium containing 2% fetal bovine serum, 7.5 mM L-glutamine, 5 ng/mL FGF, 50 μg/mL ascorbic acid, 1 μg/mL hydrocortisone hemi succinate, 5 μg/mL insulin and antibiotics/antimycotic (Growth Medium or GM); GM did not contain phenol red. The cells were incubated

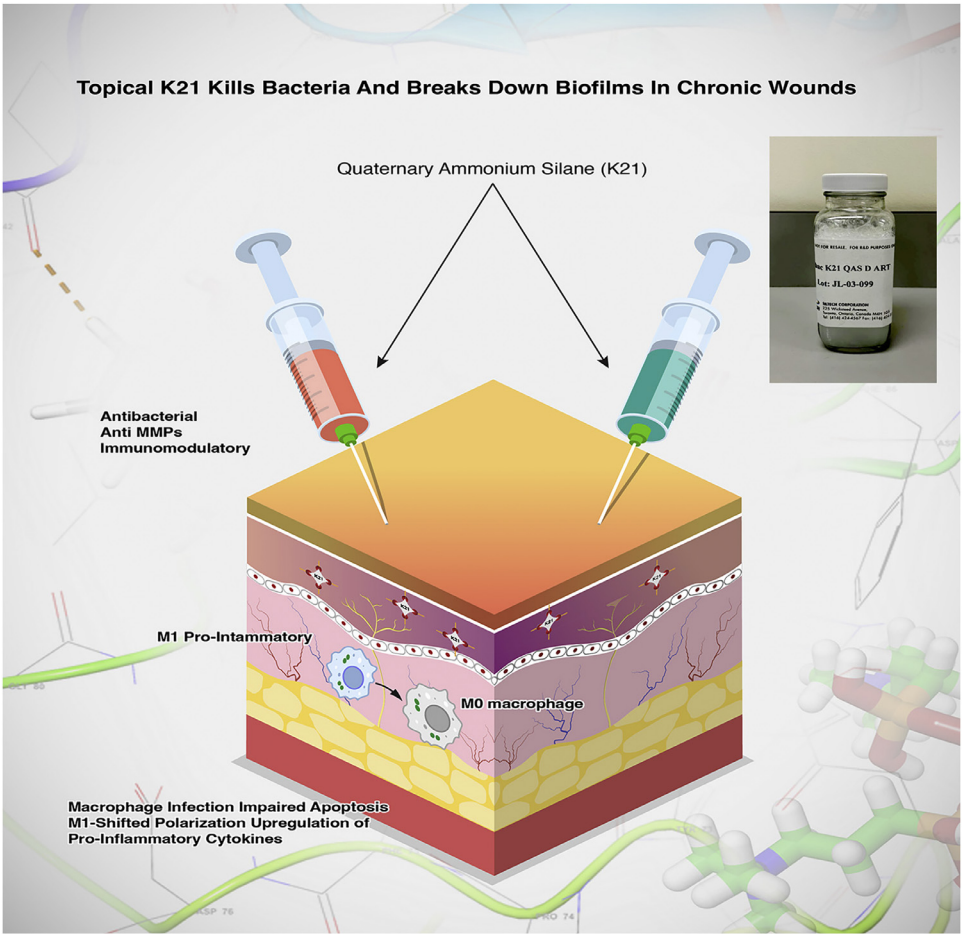

Fig. 1 – The K21 molecule belongs to a class of positively charged surfactants that exhibit an electrokinetic phenomenon when in contact with a solid-liquid interface. This phenomenon occurs due to the existence of hydrophilic and lipophilic groups inside the surfactant molecules. K21 can be injected into the wound area for sufficient absorption. This general representation is of macrophage polarisation via a process through which macrophages obtain distinctive functional features as a response to certain stimuli from their niche. This process has a critical impact in tissue repair and maintenance of tissue homeostasis. The chemical possesses well-documented properties for eradicating germs and disintegrating biofilms in persistent wounds. Inset K21 bottle.

at 37 ± 2°C in a humidified atmosphere (5% CO_2). After reaching 60 to 80% confluency, cells were dislodged from the flask surface using 0.05% trypsin. Cells were centrifugated for 12 min and seeded into flasks (8°C). Cell migration was measured using the QCMTM 24-well colorimetric cell migration assay (Millipore catalogue number ECM 508, EMD, Rockville, MD, USA).

Test procedure

Negative controls. Growth Control (GC): Untreated GM.

Solvent Control (SC): Ethanol (100%) was used to prepare the test item dosing formulation solvent control.

Preparation of cells. On the day of treatment, the number of cells were counted using trypan blue exclusion and a cell suspension of approximately 0.5 × 10^6 cells/mL were prepared in growth medium. For the migration and proliferation assay, the inserts (upper chambers) were seeded with 300 μL of cells (approximately 1.5 × 10^5 cells/insert) and placed in a 24-well migration and XTT plate (lower chambers) respectively.

Preparation of test item dilutions. On the day of treatment, a test item stock solution was freshly prepared by accurately measuring the appropriate amount of test item and adding the appropriate amount of ethanol.

Treatment. For the migration assay, each treatment diluted in growth medium was added to the lower chambers of the migration plate in duplicates (500 μL per well). For the proliferation and XTT assay, each treatment diluted in growth medium and added to the cells in duplicate (500 μL per well). The plates were covered and incubated at 37 ± 2°C in a humidified atmosphere containing 5% CO_2 for 24 h.

Assay analysis. For migration analysis, the extracted dye (100 μL per well) was transferred into a clean 96-well plate. The plate was read at 560 nm using a spectrophotometer. For cell

proliferation assay, the cell proliferation kit (XTT) and phenazine methosulfate (PMS) was handled in a darkened room with gold lighting. Any bubbles in the clear 96-well plate were removed prior to spectrophotometry.

Cell Line

The human peripheral blood mononuclear cell line, SC (CRL-9855 #LOT: 61834527), was acquired from ATCC.

Analysis of Macrophage Phagocytosis

The cells were immobilised using 3% glutaraldehyde for 24 hrs and then washed with phosphate buffer. They were later fixed using 1% osmium tetraoxide (1 hr) at a temperature of 4° C. Subsequently, the cells underwent further rinsing with distilled water and were then stained with a 1% solution of uranyl acetate for 1 hour. The cells underwent successive dehydration by being exposed to ethanol at concentrations of 50%, 80%, 90%, and 100%. Following this, the cells were subjected to ethanol solutions containing epoxy resin at a concentration of 66.7%. Subsequently, the cells were immersed in resin for a duration of 24 hrs (70°C) to prepare them for sectioning using an ultramicrotome. The sections were examined using a voltage of 100 kV (JEOL 3010 TEM, JEOL USA, Peabody, MA, USA).

Data Preprocessing and Spectral Analysis: The Raman Affect

The cultured macrophages were attached to the cover slips and activated with LPS. They were then placed in a desiccator for 24 hrs to remove moisture. The Raman spectra (ULWD) were collected using the Renishaw RM-2 Raman microscope equipped with an Olympus (BH-2) 20 objective lens. The specimens were subjected to stimulation using a 785 nm diode laser, with a laser power setting of 5 mW, covering a wavelength range of 200 cm^{-1} to 3200 cm^{-1}. The ultimate spectrum was generated by merging 40 photos and applying baseline correction using a fifth-degree polynomial function within the Origin Pro 2024b software.

Macrophage Polarisation and Activation for Exposure to QAS/K21

The SC human peripheral blood mononuclear cell line (CRL-9855 #LOT: 61834527) was acquired from ATCC (PCS-800-011). To achieve a concentration of 2×10^5 cells per flask, the cells were enumerated and cultivated using Iscove's Modified Dulbecco's Media (IMDM; ATCC, Lot:63331110-Manassas/VA). The solution was supplemented using 10% FBS, 0.1 mM hypoxanthine and added with 0.05 mM 2-mercaptoethanol and 0.016 mM thymidine. After 2 days, the cells were subjected to phosphate buffered saline rinsing (PBS). The cells were harvested at a concentration of 1.5×10^4 cells/cm^2 for further Raman experiments.

K21 Exposure

For the antimicrobial exposure, DMEM was utilised, with the addition of 0.1 ml administered gradually for subsequent tests.

Macrophage Exosomes

The quantification of macrophage exosomes was performed using microBCA protein assay Kit (Beyotime, China). The morphology was evaluated on uranyl acetate, $UO_2(CH_3COO)_2$, stained grids and imaged using 100 kV voltage (JEOL 3010 TEM, JEOL USA, Peabody, MA, USA). Exosome structures were identified at 300 nm scale utilising the TEM.

Immunofluorescence Staining

CD 206 (mannose receptor) (Catalog # PA5-46994; ThermoFisher Scientific, USA) was employed for immunofluorescence staining to assess M2 polarisation. Following a 24-hour incubation period, the cells were immobilised using a 4% paraformaldehyde solution for 15 minutes (24°C). The cells were subsequently cultured with rabbit anti-CD206 antibodies (1:200) for an extended period (4°C). Following a 24-hour period, the cells underwent saline rinses and were then stained with goat anti-rabbit AlexaFluor594-conjugated antibody (1:200, Abcam, USA) in a dark room for 1 hour. Following an additional five-minute washing step, the nucleus was stained with DAPI for a duration of 10 minutes. Ten images for each specimen were then captured using a confocal laser scanning microscope (Olympus FV1200) with illumination provided by a 484 nm laser and then analysed using bioimage software version 2.0, developed in Malmö, Sweden.

Scanning Electron Microscopy

The morphologies of macrophage cells were studied using a high-resolution field emission scanning electron microscope (Auriga Compact, Zeiss, Germany) with an accelerating voltage of 10 kV. Before conducting any scanning electron microscopy (SEM) investigations, all specimens underwent a process of sputter-coating with Pd ion sputtering (EMACE600, Leica, Germany). Two dentin discs were utilised to cultivate cells for a duration of 24 hrs. Following this, the discs were fixed utilising a 4% glutaraldehyde solution in PBS for a period of 4 hrs at room temperature.

Morphometric and Microscopic Analysis of Partial Thickness Burn Wound Healing

This study was a 3-month experimental animal trial. This study was conducted and approved at the Animal House and Oral Biology Department of Akhtar Saeed Medical and Dental College in Lahore and the ARRIVE guidelines were followed for animal usage.[14] A total of twenty-one male rabbits, with weights ranging from 750 to 1000 g, were utilised for the purpose of this investigation. Rabbits that were both diseased and female were not included. The Institutional Review Board of Akhtar Saeed Medical and Dental College, Lahore, Pakistan, accepted the experiment (IRB #: M-23/148/- Oral Biology). Next, the animals were measured for weight and then rendered unconscious by administering an intramuscular injection of 75 mg/kg ketamine (Troy Laboratories, Glendenning, Australia) and 15 mg/kg xylazine (Troy Laboratories, Glendenning, Australia).

The dorsal skin was shaved with clippers and additionally, the small hair was removed by applying a commercial hair removal cream (VEETTM; Reckitt Benckiser, NSW, Australia) as per guidelines. Thermal burns were produced with the help of a heating device manufactured for this purpose (Fig 6). Two wounds were created on the upper back on both sides of the midline, with 8 cm from the central point of each wound.

In the control group no treatment was applied while in the experimental group, 0.46% K21 (2 mL) was dropped on the wound area with the help of a dropper every day, and the movement of the animal was restricted for 5-10 min for sufficient absorption. For morphometric analysis, images of the wound were captured by the camera of iPhone 15 Pro Max (48MP) on days 1, 8, 11, 14, 18, and 21. The wound area was measured using ImageJ, version 1.54g. The mean value was taken at the magnification of 5X. The data was presented as means± SD and subjected to independent samples t-test, keeping the confidence interval at (95%) and significance level at (≤ 0.05). analysis was performed using SPSS software, version 27 (IBM, Armonk, NY, USA). For histological analysis, animals were sacrificed on days 14, 18, and 21, and full-thickness skin was harvested from the previously injured area, samples were fixed with 10% formaldehyde and then processed and sectioned 3-5 μm using a Leica microtome. The sections were stained with hematoxylin and eosin stain and the histological images were captured using a Nikon E200 microscope and camera. The following variables were observed and analysed:

1. The epithelial thickness over the injury site was evaluated on a scale of 1 to 4.[1 (0-2 cell layers), 2 (3-5 cell layers), 3 (6-10 cell layers), and 4 (> 10 cell layers)].
2. Rete ridges were evaluated based on presence (1) and absence (0).
3. The inflammatory reaction near the injury site in the epidermis and dermis tissue was based on the inflammatory cell number [Mild (< 10 inflammatory cells), Moderate (10-50 inflammatory cells), (Severe (>50 inflammatory cells)][15].

The slides were immersed in xylene and ethanol to remove any impurities before being placed in Bouin's solution at a temperature of 60°C for a duration of 45 minutes for Masson's trichrome staining. Masson trichome stain (Cytoplasm – red, Muscle – red, Collagen – green, and Nuclei – dark brown). The newly formed collagen fibres were evaluated based on the orientation (vertical-0, horizontal-1).

Triacylglycerol Accumulation within Macrophages: Generation of M1 and M2 states to Evaluate Triacylglycerol

M1 and M2 states in macrophage cells were stimulated by utilising ultrapure lipopolysaccharides (LPS; InVivogen) and 20 ng/mL interferon-y (IFNγ; Pepro Tech) for M1 polarisation, and 20 ng/mL IL-4 (Pepro Tech) for M2 polarisation, in differentiation medium for a duration of 24 hrs. The LCMS/MS analysis was conducted using a 4000 Qtrap mass spectrometer (AB Sciex) equipped with an Agilent 1290 series HPL Canda ZORBAX eclipse plus C18 column (2.1 × 100 mm x 1.8 μm, Agilent). The column temperature was maintained at 60°C.

Cell Preparation and RNA Extraction for Real Time RT-PCR

A total of 10,000 cells were placed in each well of a 96-well plate and incubated for 24 hrs. The medium was then withdrawn and replaced with an adequate concentration of HOCl. The total RNA was isolated using TRIzol (GIBCO/BRL Life Technologies) and then purified using the RNase-Free DNase Set and RNeasy Mini kit (Qiagen, Valencia, CA). The genes exhibiting differential expression were compared across all groups by utilising the GeneChip IVT labelling kit to bio label cDNA transcribed to cRNA. A total of fifteen micrograms of cRNA, which were labelled, were subjected to hybridisation on an Affymetrix Mouse Genome 430 2.0 Array at a temperature of 45°C for a duration of 16 hrs. Following the washing process using the GeneChip Fluidics Station 450, the arrays were scanned using a GeneChip 3000 scanner. Intensity values were then retrieved from the CEL file using Array Assist software (Stratagene, La Jolla, CA). The process involved the reverse transcription of the whole RNA using MuLV reverse transcriptase primers. The SYBR Green PCR Kit from Applied Biosystems in Carlsbad, CA was utilised for quantitative real-time RT-PCR analysis. The measurement of fluorescence in real-time was performed using an ABI PRISM 7700 Sequence Detector manufactured by Applied Biosystems.

Results

The human primary gingival fibroblasts (PGF) results are summarised in Table 1, Fig 2 and Fig 3. After 24 hrs of treatment, K21 increased the migration of PGF cells when compared with the concurrent SC (Fig 2 and Fig 3). The mean absorbance at 560 nm (A560) for the SC was 0.651, and the mean A560 for K21 ranged from 0.964 to 0.755 (Table 1). (Supplement Fig 1). The increase in migration following K21 treatment was dose-dependent, with 6.25 and 12.5 μg/mL showing A560 values greater than the SC (Fig 2). The mean A560 for the SC was 0.651, and the mean A560 for K21 ranged from 0.829 to 0.397 (Table 1). K21 decreased PGF proliferation in a dose-dependent manner confirming appropriate treatment up to a cytotoxic concentration; the cytotoxicity was more pronounced with K21 lot AP10-069. The proliferation (mean A450) of the SC was 0.647, the mean A450 of K21 lot AP-6- 061 ranged from 0.634 to 0.460, and the mean A450 of K21 lot AP10-069 ranged from 0.626 to 0.118 (Table 1).

Raman spectroscopy was used using a spectral range of 700-1800 cm^{-1}. The mean spectra exhibited significant Raman peaks at 1035 cm^{-1}, 1577 cm^{-1}, 1662 cm^{-1}, 860 cm^{-1}, 1127 cm^{-1}, 1305 cm^{-1}, 1442 cm^{-1}, and 1658 cm^{-1} (Fig 4A-B). The evaluation conducted for each Raman band seen during the transition from M1 to M2 was based on already published material. The frequency of 1035 cm^{-1} corresponds to the stretching of the C-C bond, which is associated with the lipid signatures seen at 1442 cm^{-1} (representing the deformation of CH2CH3) as shown in Figure 5. Furthermore, the presence of nucleic acid and amino acid fingerprint area was indicated by 1577 cm^{-1} and 860 cm^{-1} wavenumbers respectively, exhibiting several noteworthy alterations (Fig 4B). The mean Raman spectra at 1662 cm^{-1} and 1658 cm^{-1} corresponded to the lipid and collagen areas of the macrophage assessment, which included

Table 1 – Summary of Cell Migration and Proliferation Tests in Human Primary Gingival Fibroblasts

Treatment	ID	Concentration (μg/mL)	Cell Migration %				Cell Proliferation %			
			N1	N2	Mean	SD	N1	N2	Mean	SD
Growth Control	**GC**	0	1.515	1.147	1.331	0.260	0.679	0.654	0.666	0.017
Solvent Control	**SC**	0	0.896	0.405	0.651	0.347	0.624	0.669	0.647	0.032
K21 lot AP-6-061	**X1**	1.56	0.732	0.920	0.826	0.133	0.658	0.610	0.634	0.034
	X2	3.13	0.819	0.793	0.806	0.018	0.623	0.602	0.613	0.015
	X3	6.26	0.837	0.673	0.755	0.116	0.629	0.623	0.626	0.004
	X4	12.5	1.032	0.895	0.964	0.097	0.605	0.589	0.597	0.011
	X5	25.0	0.958	0.831	0.895	0.090	0.448	0.472	0.460	0.017
K21 lot AP10-069	**Y1**	1.56	0.333	0.461	0.397	0.091	0.612	0.640	0.626	0.020
	Y2	3.12	0.621	0.619	0.620	0.001	0.607	0.624	0.616	0.012
	Y3	6.25	0.733	0.628	0.681	0.074	0.618	0.630	0.624	0.008
	Y4	12.5	1.059	0.598	0.829	0.326	0.532	0.506	0.519	0.018
	Y5	25.0	0.764	0.424	0.594	0.240	0.139	0.097	0.118	0.029

characteristic protein markers. The mean Raman spectra of the M0, M1, and M2 macrophages displayed slight variations in the strength of different peaks. When comparing the average spectra of M1 and M2 profiles, no shifts in the positions of the peaks and no significant alterations in the intensities of the peaks were observed. The spectrums depicted the average of 100 separate recordings acquired from the macrophage subgroups in each specimen, revealing notable alterations. The main component analysis of the Raman data for all macrophage subset phenotypes supported the results that characterised the phenotypes and characteristic polarisation, as well as the representative biochemical variations between the cell groups (Fig 4C). The positive data showed a rise in the Raman signals, while negative loadings suggested a drop in

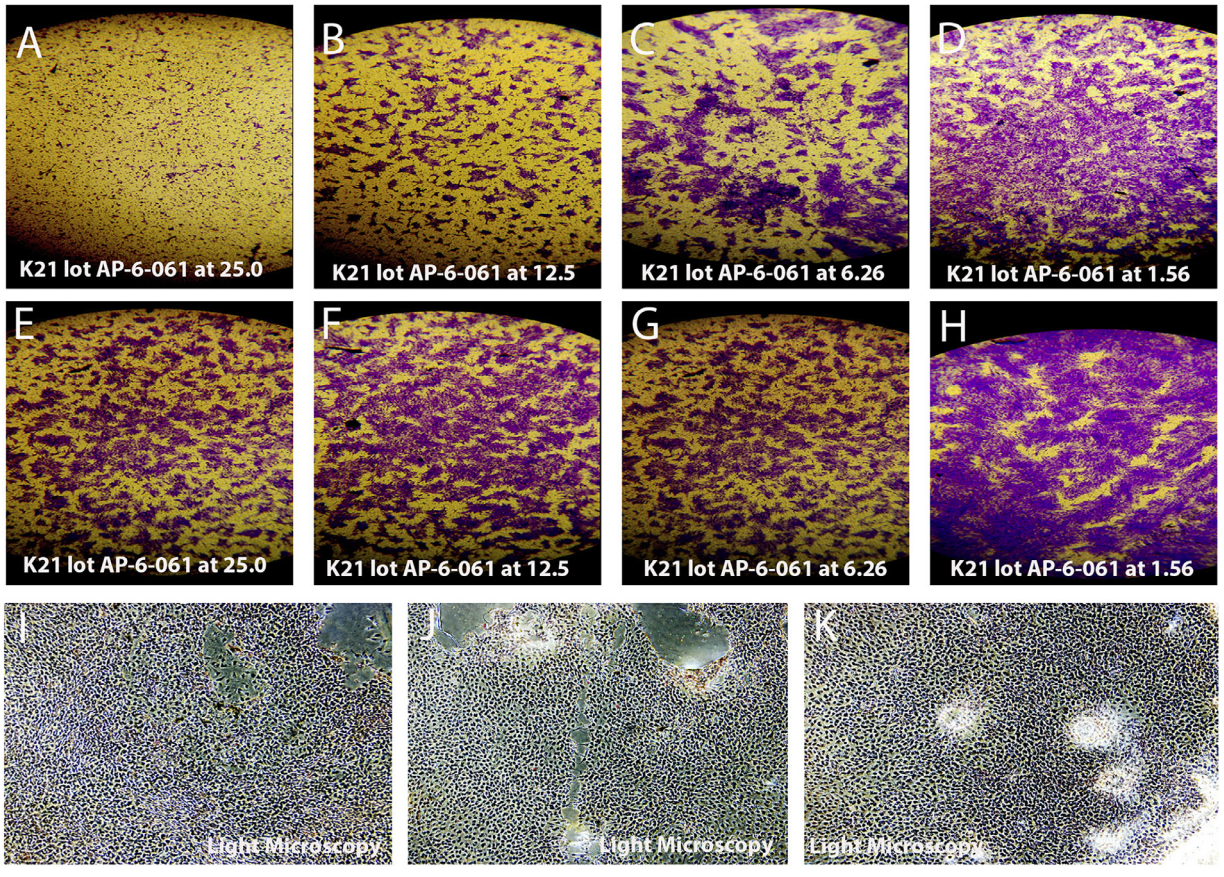

Fig. 2 – The ability of two lots of K21 to influence the migration of human primary gingival fibroblasts (PGF) was evaluated in this study. Ethanol was included as the solvent Control (SC) and undiluted GM was included as the Growth Control (GC)3. K21 lot AP-6-061 was evaluated at 25.0, 12.5, 6.26, and 1.56 μg/mL. After 24 hrs of treatment, K21 increased the migration of PGF cells when compared with the concurrent SC. (A-H) Representative pictures of the fibroblastic proliferation are shown as the images were quantitatively analysed. (I-K) The light microscope merged image is to show the proportion of proliferating cells after K21 treatment.

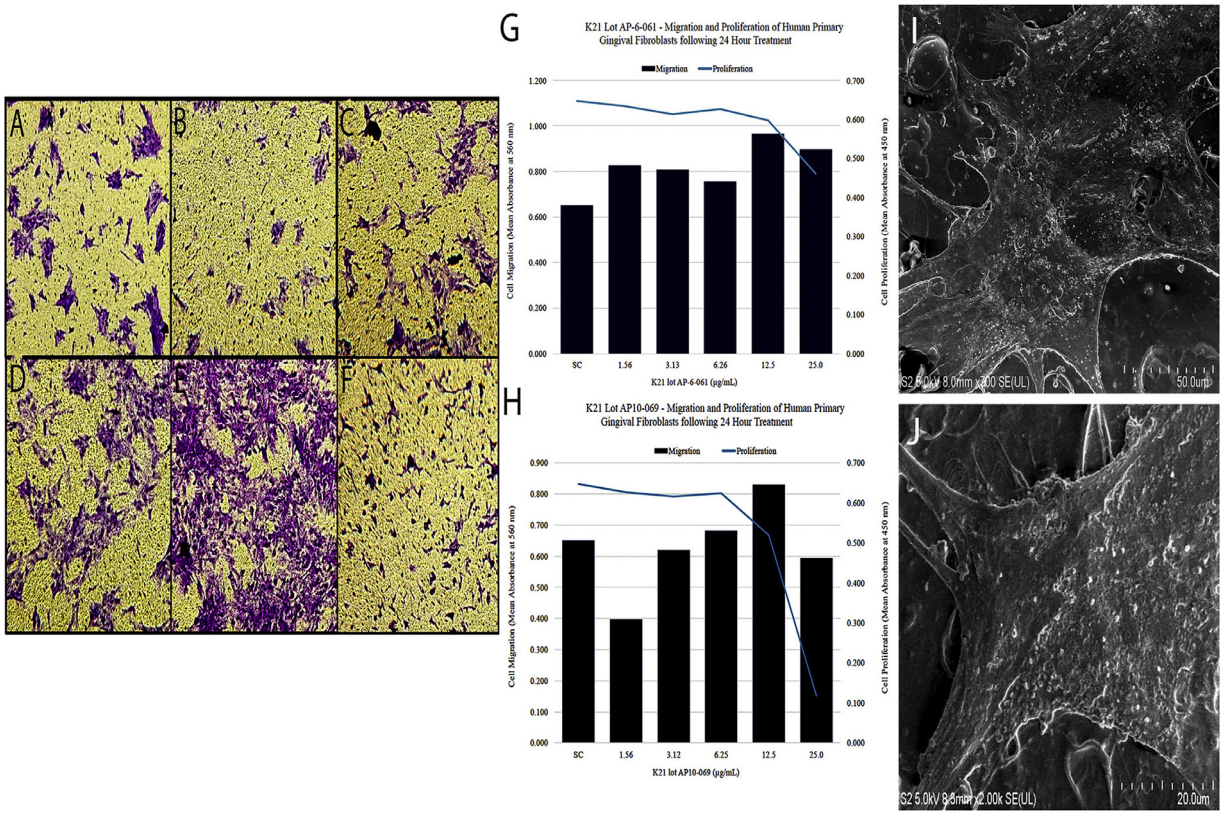

Fig. 3 – (A) Photograph of stained inserts showing cells that migrated through the membranes. (B-F) Photomicrographs of stained cells that migrated through the membranes following K21 treatment. (G) K21 Lot AP-6-061 - migration and proliferation of human primary gingival fibroblasts following 24-hour treatment, (H) K21 Lot AP10-069 - Migration and proliferation of human primary gingival fibroblasts following 24-hour treatment. (I-J) Fibroblastic growth amongst K21 treated specimens.

the M1 state (Fig 4D), which ultimately led to the transition to the M2 state. The scores reflected the spread of samples in perpendicular directions ***(data not shown)***.

As shown in Figure 5A-C, TEM revealed rounded morphology of the exosomes within K21 groups *(arrow)* enabling the clustering and tethering with K21 groups (0.46%-0.1%). There was upregulation of autophagy markers (Fig 5D) CD206 in macrophages treated with K21 (Fig 5E-F) groups compared with the control group (Fig 5D). The highest concentration of markers occurred at the concentration of 0.46% K21 groups. Immunofluorescent staining also confirmed higher expression of CD206 in K21 treated groups (Supplement Fig 2) compared with the control groups. The scanning electron images revealed the M2 shaped macrophages while the control macrophage appeared spherical **(Fig S1C)**. The TEM images showed uptake of K21 within the macrophages (Supplement Fig 2A, D, E) with normal functioning cell organelles (Supplement Fig 2F). The M0-macrophages were observed to be small and ovoid cells (Fig 5G-I) which were devoid of any cytoplasmic extensions. Some of the cells appeared to have a fusiform morphology. Most of the M1 macrophages had a fusiform shape with elongations present within cytoplasmic bodies and extensions visible on the cell surface. M2 cells appeared to have a mix of different morphologies with fusiform and elongated bodies and massive cytoplasmic extension (Fig 5K-L). Both poles appeared exaggerated.

After thermal burn damage, there was a significant swelling which caused the wounds to appear uniformly white (Fig 6). No blister was noticed and the demarcation between the wound region and the normal skin was distinct, indicating a deep partial-thickness burn. The burn wound located on the left side of the animal was subjected to K21 treatment, while the opposite side was maintained as the control side. On the first day following the burn, swelling persisted, with formation of a small scab noted in the vicinity of the wound. By day 3, the whole area of the burnt skin was completely covered with a firm layer of crust. On day 8, the scab was detached with visible signs of healing and contraction by day 11. By the 14th day, the area continued to decrease in size, while maintaining a layer of skin. By day 21, the wound area in the control group was modest, but complete epithelialisation had not occurred. In contrast, the K21-treated group had completed complete healing by this time (Fig 6). There were statistical differences ($p<0.05$) in the rate of wound area contraction between day 8 and day 21 (Supplementary Table 1 and Fig 6).

The histological analysis performed on day 18 showed incomplete wound coverage with absence of hair follicles within the K21 groups. The newly formed rete ridges were densely packed and present within the papillary layer. There were horizontally oriented collagen fibres present in the dermis, with mild inflammatory response in presence of

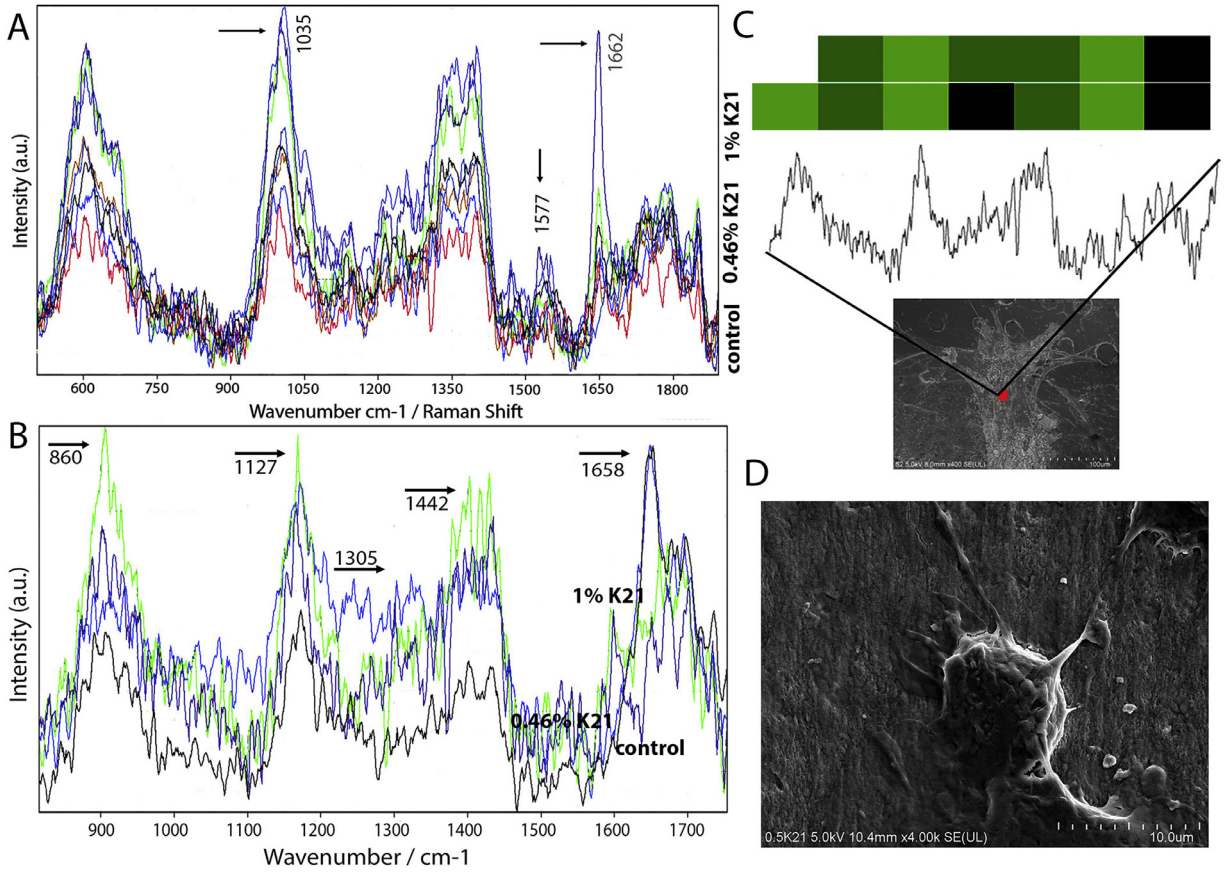

Fig. 4 – (A-B) Macrophage polarisation states were evaluated using Raman spectroscopy within the spectral range of 700 to 1800 per cm. The average spectra showed appreciable Raman peaks corresponding to 1035 per cm, 1577 per cm, 1662 per cm, 860 per cm, 1127 per cm, 1305 per cm, 1442 per cm, and 1658 per cm. The average Raman spectra of 1662 per cm and 1658 per cm represented the lipid and collagen regions of the (D) macrophage evaluation, a collection that consisted of typical protein markers. The mean spectra exhibited significant Raman peaks at 1035 per cm, 1577 per cm, 1662 per cm, 860 per cm, 1127 per cm, 1305 per cm, 1442 per cm, and 1658 per cm. The presence of nucleic acid and amino acid fingerprint area was indicated by the wavenumbers 1577 per cm and 860 per cm, respectively, exhibiting several noteworthy alterations (B). The positive data showed a rise in the Raman signals, while negative loadings suggested a drop in the M1 state (D).

neutrophils and lymphocytes. In Masson trichome stained sections, the collagen fibres appeared mature in K21 group and were horizontally oriented inside the dermis (yellow arrows), representing healthy tissue healing. The control groups revealed incomplete wound coverage, loosely packed vertically oriented collagen fibres, and a severe acute inflammatory response with dominant neutrophils cells present inside the dermis and the epidermis (Fig 6) (Table 2). The collagen fibres appeared vertically oriented and less organised within the dermis (yellow asterisk) with greater amount of granulation tissue (Fig 7).

On day 21, keratinised squamous epithelial (6-10 layers) layers with newly developed rete ridges, densely packed horizontally oriented collagen fibres were observed in K21 groups ($p<0.05$). The collagen fibres were horizontally oriented, condensed and well organised. The wound areas had not completely healed within the control group and rete ridges were absent, with loosely packed horizontally oriented collagen fibres and moderate inflammatory response in presence of neutrophils (Fig 6) (Table 2). The collagen fibres were mixed (vertical as well as horizontal) with disorganisation and granulation tissue beneath the wound surface (*yellow asterisk*) (Fig 7). Pathological fibrosis was not present in any of the specimens as rabbits had great regenerative capabilities but accumulation of granulation tissue with less oriented collagen fibres in the control group lead to delayed healing. For incisional wound morphometry and histology, the wound was 3 cm in length. On day 3 after the incision, the wound contraction was apparent with healing in the K21-treated group (black arrow) while the wound was wide open in the control group. On the 11th day, the area was filled with thick epidermis with a gap in the incisional margins within the control groups. Therefore, complete healing was achieved in the K21 treated group. After day 11, epithelial defects were filled (>6 layers) (black arrow) in K21 groups, with vertically oriented collagen fibres that were condensed, well organised, and exhibiting mild inflammatory reaction. The epithelial defects had not been filled (black arrow) and there was severe inflammatory reaction present at the incision site within the control groups (Supplementary Fig 3).

Supplementary Fig 4A represents the heatmap of genes (rows) and sample (column). The colour and intensity of the

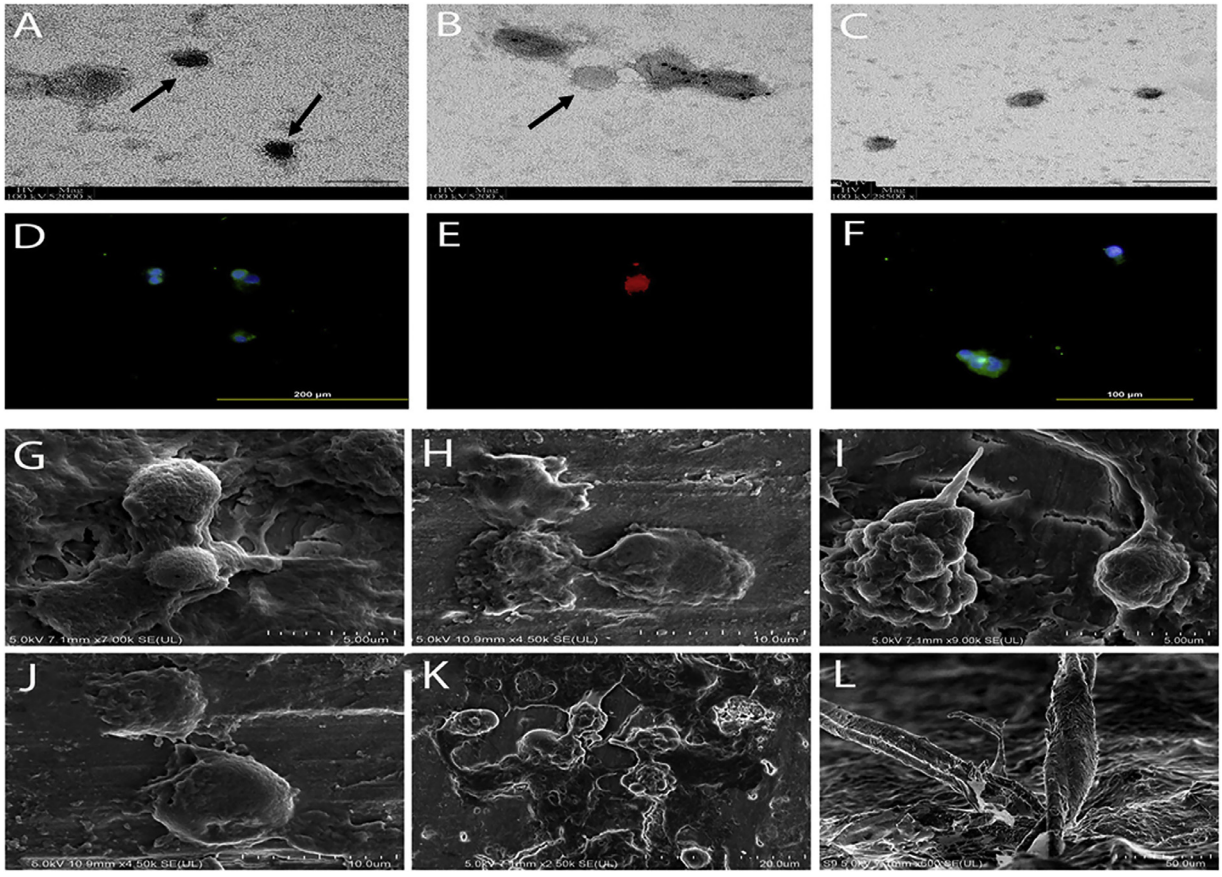

Fig. 5 – Transmission electron microscopy (TEM) revealed rounded morphology of the exosomes within K21 groups (*arrow in A, B*) enabling the clustering and tethering and release peaking with K21 groups (0.46%-0.1%). There was an upregulation of autophagy markers CD206 in macrophages treated with 0.46% and 1% K21 (E-F) groups compared with control group (D). After 24 hrs of cell culture and K21 exposure, FESEM was performed to observe changes in cell morphology. The M0-macrophages were observed to be small and ovoid cells (G-I) which were devoid of any cytoplasmic extensions. Some of the cells appeared to have a fusiform morphology. The majority of the M1 macrophages also appeared fusiform with elongations within cytoplasmic bodies and extensions appearing on the cellular surface. M2 cells appeared to have a mix of different morphologies with fusiform and elongated bodies and massive cytoplasmic extension (K-L). Both poles appeared exaggerated.

tiles represent changes (not absolute values) of gene expression. Supplementary Fig 4A heatmap represents the hierarchical clustering of the inflammation related genes species in the control, K21 and LPS groups, colored by abundance intensity; the identified inflammation related genes are represented by each line on the graph. The scale ranging from -4 to +4 is color-coded from blue to red, indicating decreasing to increasing levels of abundance, respectively. This colour scheme represents lower cytokines and an anti-inflammatory state. Supplementary Fig 4B depicts the differential gene expression, namely the volcano plot of RNA-seq/DNA-seq expression data before and after differentiation. The graph uses colored dots to represent genes that exhibit differential expressions with an absolute log fold change of more than 1 and a p-value less than 0.05. Black dots, on the other hand, indicate genes that do not match these requirements. The horizontal line represents a significant value of $p<0.05$ (K21 versus LPS) that has been adjusted using the Bonferroni correction. The dashed vertical lines define the minimum fold-change for the genes that are expressed with the greatest difference. The top 29 GO functional categories for each most-differentially-expressed gene set (either upregulated or downregulated) following treatment are listed on both sides.

Supplementary Fig 4C displays the differential gene expression using a volcano plot, which shows the changes in RNA-seq/DNA-seq expression data before and after differentiation. The graph displays colored dots to represent genes that exhibit differential expression with an absolute value of the logarithm of the fold change more than 1 and a p-value less than 0.05. Conversely, black dots indicate genes that do not match these requirements. The horizontal line represents a significant value of p0.05 (LPS vs control) that has been adjusted using the Bonferroni method. The dashed vertical lines define the minimum fold-change for the genes that are expressed with the greatest difference. The top 29 GO functional categories are displayed for each most-differentially-expressed gene set, indicating whether they are upregulated or downregulated. Gene Ontology (GO) term enrichment is a

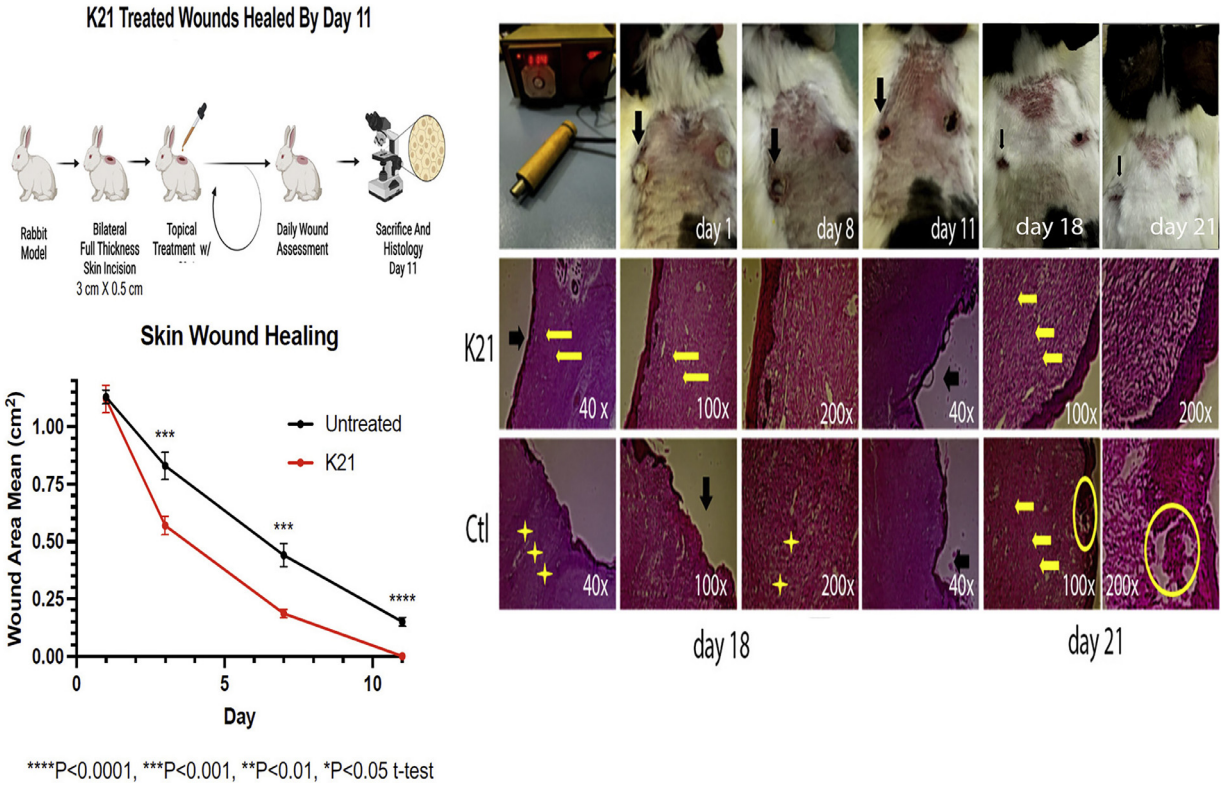

Fig. 6 – Healing of thermally induced skin burns. After the injury, severe edema was observed, resulting in uniform white wounds. No blisters were observed and the edges between the wound area and the normal skin were clear, depicting it was a deep partial-thickness burn. Black arrows represent the K21-treated area. Photomicrographs (H&E staining) of thermally induced skin burn on day 18. Wound area (black arrow), collagen fibres (yellow arrows), and inflammatory cells (yellow asterisks). There was the closure of the wound area with the formation of rete ridges in the papillary layer, densely packed, horizontally oriented collagen fibres were present in the dermis and mild inflammatory response within all K21-treated specimens. In the control group, there was incomplete wound coverage, loosely packed vertically oriented collagen fibres, and severe acute inflammatory responses with neutrophils as dominant cells were present in the dermis and the epidermis. On day 21, in the K21-treated group, there was complete wound coverage with keratinised squamous epithelial (6-10 layers) (black arrow) with newly developed rete ridges and densely packed horizontally oriented collagen. A thin layer of epidermis was formed at the wound area. The dermis was filled with plenty of fibroblasts and blood vessels, showing well-developed granulation tissue in the control group.

method used to analyse collections of genes by utilising the Gene Ontology categorisation system. This approach categories genes into predetermined groups based on their functional features. The result of the study usually consists of a list of GO keywords, arranged in order, with each phrase being linked to a corresponding p-value. Supplementary Fig 5 displays the results of the Gene Ontology (GO) enrichment analysis using KEGG pathways for a dataset consisting of 29 genes associated with inflammation. KEGG pathways are sorted based on their fold enrichment levels. The processes with the highest significance are indicated in red, while the processes with lower significance are indicated in green based on the log10 (FDR) values. The graph displays larger dots to represent a higher quantity of genes that are related to the top 50 pathways linked to 29 inflammatory genes. The first two routes are crucial for gene activity, as seen in Supplementary Table 2.

Figure 8A displays a Venn diagram illustrating the quantity of genes identified in five distinct pathways. Every set symbolises a distinct phase of growth or progress. The numbers in each intersection indicate the count of genes that have been identified with at least one read (gene tag) in these separate sets (intersections). The topic is the interplay between cytokines and cytokine receptors, specifically in the context of the colour green. The topic is the relationship between cytokines and the inflammatory response pathway. Pink: The medical term for pertussis. The yellow colour represents the route of cytokine generation. Orange: route of signaling controlled by cytokines (K21). Protein-protein interactions (PPIs) are precise physical contacts that occur between two or more protein molecules because of biochemical activities driven by interactions including electrostatic forces, hydrogen bonding, and the hydrophobic effect. Protein-protein interaction is crucial for predicting the function of a target protein and the capacity of compounds to act as drugs. The ensuing phenotypic functions are achieved by a series of interactions between genes and proteins. An investigation of the protein-protein interaction (PPI) network was

Table 2 – Histomorphometry analysis of burn wound comparing control and K-21 treated group on different days.

	Day 14 (p-value)	Day 18 (p-value)	Day 21 (p-value)
Epithelial thickness	4.5	4.5	0.000*
Rete ridges	-	-	0.014*
Collagen fibres	-	-	0.014*
Inflammatory reaction	0.000*	0.000*	0.000*

Blank cells represent constant value, so no statistics were computed

conducted using the STRING database, focusing on differentially expressed genes. The 29 genes that showed differential expression were included into the STRING database for analysis of protein-protein interactions (PPI), resulting in the generation of a PPI network. The plug-in MCODE in Cytoscape was used to analyse the three main clusters of subnetworks. The nodes within each cluster were then entered into the STRING database to produce the protein-protein interaction (PPI) subnetworks (Fig 8B-C) (K21).

An exact observation was made of M1 macrophages exhibiting significant and elevated quantities of TGs, in line with the findings of the current research. There was a notable variation in the TG profiles of M1 and M2 groups. The triacylglycerols, present in K21 treated M2 macrophages, were mostly saturated, with over 75% of them being totally saturated. They did not contain any double bonds in the fatty acyl chains. Conversely, all groups observed in M1 macrophages had a greater percentage of TGs containing unsaturated fatty acids (double bonds) (Supplementary Fig 6 A).

Discussion

Cytotoxic analysis against gingival fibroblastic cells is performed to determine the effect on specific cell line. Of note, the *in vitro* test conducted may have overestimated the cytotoxic effect of the K21 material used. The effects were seen with minimal concentration of K21 antimicrobial used against the higher concentration of eluates. K21 antimicrobial induced migration in human primary gingival fibroblasts at the minimal concentration used. The increase in fibroblast migration following K21 treatment was dose-dependent, with 6.25 and 12.5 μg/mL showing A560 values greater than the SC (Fig 2-3). The cytotoxic analysis was performed against fibroblasts because of the original site of these cells (gingiva) and their possible proximity in clinical conditions. In addition, ISO further recommends the use of fibroblasts as a test cell line for cytotoxicity.[16] The findings reported herein for fibroblast viability suggest that K21 tested with a specific concentration did not present cytotoxicity. Cytotoxicity occurred

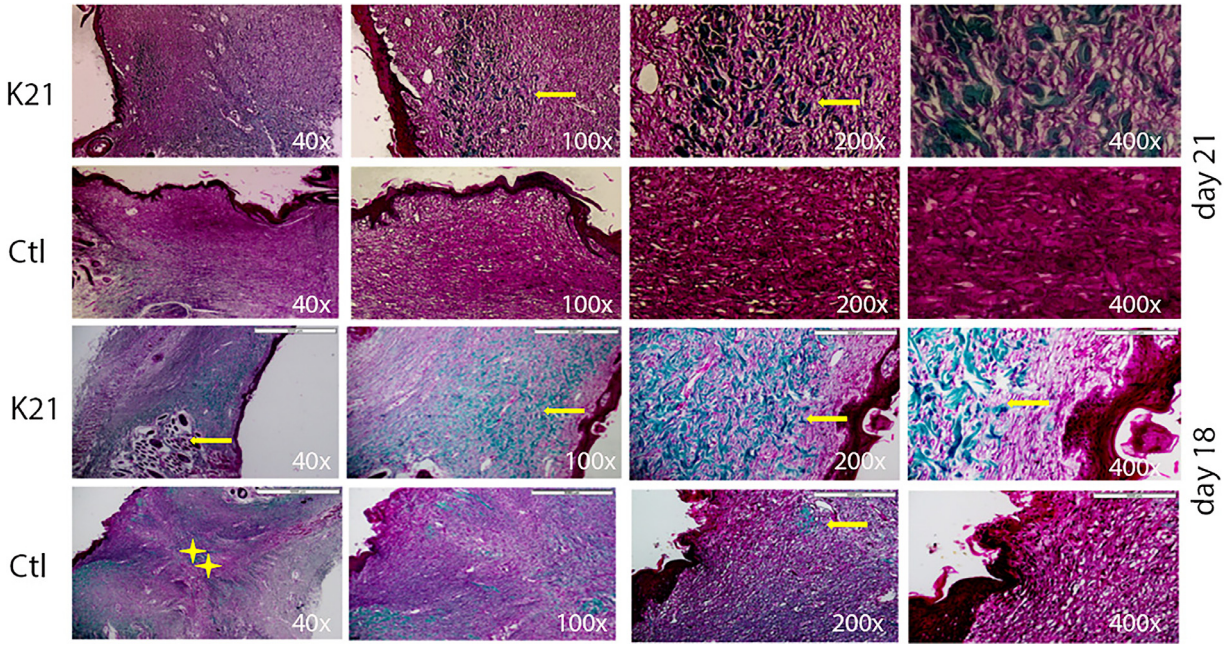

Fig. 7 – Photomicrographs (Masson trichome staining) of thermally induced skin burn. The collagen fibres were horizontally oriented in the dermis (yellow arrows), they were mature and represented healthy tissue healing, within all K21 specimens at day 18, while in the control group, vertically oriented collagen fibres were present in the dermis (yellow asterisk), they were less organised, and a greater amount of granulation tissue was present. On day 21, in the K21-treated group, densely packed horizontally oriented collagen fibres were present. In the control group, the dermis was filled with vertically oriented collagen fibres in deep tissue while plenty of fibroblasts and blood vessels, showing well-developed granulation tissue were present in the superficial layer. Original magnification 40x to 400x as indicated.

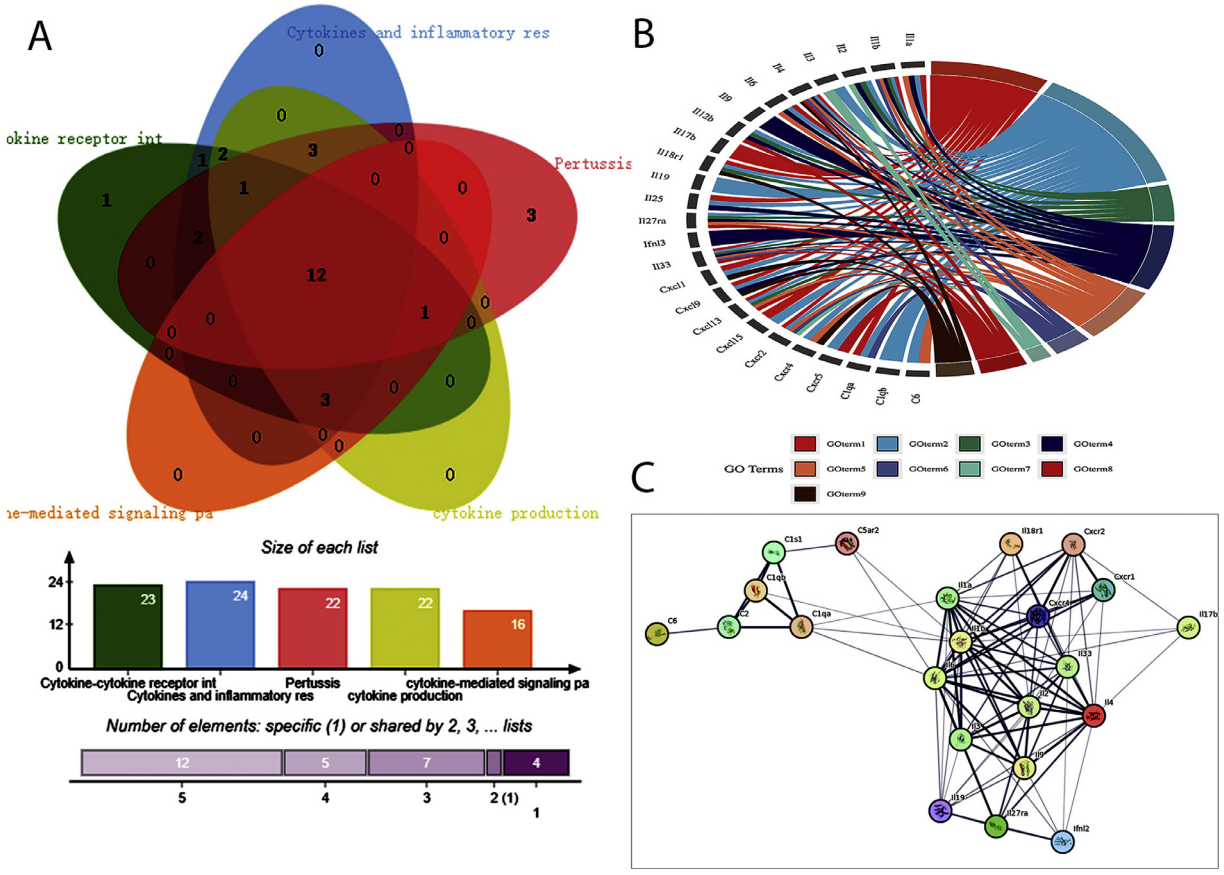

Fig 8 – (A) Venn diagram showing the number of genes detected in five different pathways. Each set represents a stage of development. (B) Nine major pathways related to 29 inflammatory genes analysed by KEGG, Go and ppi. GO:0006954 inflammatory response (C) The protein-protein interaction (PPI) network analysis of differentially expressed genes using STRING database.

only at concentrations a few times higher than what is necessary to obtain antibacterial effects. The cytotoxicity effect of the quats or quaternary ammonium may be due to the strong positive cationic charge. However, the fact is imperative that its mechanism of binding to cell walls causing the disruption via direct interaction is much less toxic in mammalian cells when compared to bacteria.[17] This may primarily be since the mammalian cells may phagocytise the antimicrobial and degrade them via lysosomal function to a degree where the toxicity is reduced.[18] This may be the reason why, even after using K21 concentrations, the reduction of fibroblast cell viability even for the highest concentration of the antimicrobial associated with their presence on the surface and/or their leaching was still small. Supplementary Fig 2 shows the effect of K21 on CD206 expression in macrophages, there was a significant increase in 0.46% K21. This result is consistent with the role of CD206 as a specific marker for M2 macrophage phenotype.[19] Immunofluorescence staining also confirmed the higher expression of CD206 in K21 treated macrophages compared with the control (Supplementary Fig 2). Moreover, the SEM images revealed the wider elongation and spindle shape of M2 macrophages while the morphology of control specimens remained spherical. These results hint towards the macrophage M0 to M2 polarisation potential of K21 treated specimens. The elongations were more observed with M1 and M2 profiles with M2 profiles demonstrating heterogeneity with cytoplasmic extensions which can be variably of different shapes.[20] Based on the images, the evaluation of M2 profiling maybe difficult and the period used may not be sufficient to show major morphological changes, although LPS was used to trigger active profiles initiating a cascade secreting proinflammatory cytokines with bactericidal/tumoricidal activities.[21] The results also are a strong indication towards the alleviation of M1 polarisation and mitigated the inflammatory phenotype of LPS-induced M1 macrophages. K21 has a virus-like surface structure mimicking virus surface topology[22] which can facilitate its endocytosis and a possible internalisation in immune cells.[16] Silica based particles are biocompatible and can show a higher rate of endocytosis being captured in macrophage lysosomes. These K21 molecules can then be degraded by the lysosomal enzymes. K21 molecules can be cytocompatibility to macrophages within which can robustly induce autophagy which inadvertently promotes M2 polarisation, reducing pro-inflammatory properties of M1 macrophages.[23] Moreover, the expression of CD 206 were characteristic hallmarks of M1 and M2 macrophages, which is also related to macrophage related IL-10 release in previous study of Daood *et al.*[24]

Similarly, the distribution and presence of exosomes showed no clear difference between the control and K21 treated macrophage cells. The size of these exosomes corresponds to the internal exosomes present within the K21 and control untreated specimens.[25] The TEM images taken further confirm the presence of donut-shaped exosomes subjected to the same separation procedure. Determining these exosome concentrations is technically challenging as it is imperative to detect and count the smallest possible exosomes and include them in the measurements. To further evaluate and confirm the identity of the isolated exosomes, and determine their concentration, additional analysis including high sensitivity fluorescence-based flow cytometry is underway.

The Raman spectra observed from M1 macrophages discovered decreased intensities of nucleic acid bands at 1557 cm^{-1} and 1162 cm^{-1}. This is primarily because of specific proteins of the phenotype due to the involvement of cell RNA.[26] Proteins bands around 1035 cm^{-1} increased specifying M1 differentiation with 1577 cm^{-1} decreasing the moment the shift is towards M2 phenotype. There is a clear indication that a change or reduction in RNA/DNA levels dominated proceedings of biochemical changes while the differentiation happened for both M1 and M2 phenotype.[27] This makes the joint analysis of Raman spectroscopy important for discrimination of biological specimens such as macrophage cells. In addition, after exposure to K21, the exposure led to brought significant changes amongst lipids and amino acids peaks further confirming that inflammation and lipid signaling are intertwined modulators of homeostasis and immunity.[28] Venosa *et a l*[29] reported a strong relationship of accumulation of phospholipids within macrophages that promote M2 polarisation. As per our current study, the phospholipid peaks appeared higher ($p<0.05$). Although the spectral differences noted between M1 and M2 were small, the Raman bands used to profile M1 and M2 profiles did show a statically significant separation between the two phenotypes.

Significant disparities in wound healing rates were seen from the first day to the eleventh day after surgery with infected burn wounds. The H & E staining technique was used to assess the inflammation and proliferation of the deep partial-thickness burn.[30] On the 11th day, the K21-treated skin tissue exhibited a morphology like that of healthy rats' skin tissue. In conclusion, the findings demonstrated that the burn sites treated with K21 had little inflammation, full re-epithelialisation, and a well-structured tissue. Wound healing, particularly in the case of burns, is a complex process. The presence of proinflammatory cytokines can stimulate the production of inflammatory cells, which in turn promote wound healing and provide protection at both the local and systemic levels. According to the figure, it can be observed that on day 11, the K21 groups had decreased levels of inflammation. This might be attributed to the anti-inflammatory properties that decrease the inflammatory reaction of wounds and accelerate the process of healing.[31] The healing process is enhanced when the collagen fibres in the K21 fibres are aligned horizontally, as indicated by the fibre orientation codes (vertical-1, mixed-2, horizontal-3). When comparing the collagen deposition in the normal tissue, there is no sign of excessive collagen fibre stacking, indicating a healthy state ***(data not shown)***.

The divergent reactions are probably a result of the phenotypic variability exhibited by the macrophages.[32] Somewhat unexpectedly, there was an increase in total TG levels of single bond saturated ones within M2 macrophages. In addition, there was a marked increase of unsaturated double bond triacylglycerol in M1 macrophage response. It is already established that various forms of lipid metabolism and pathways are rewired and programmed between macrophage polarisation states[24] which is consistent with our results in the current study, and towards sphingolipid synthesis.[33] The authors accept that the in vitro model tested for macrophage polarisation is an oversimplification of the current understanding of the phenotypes compared within the tissue resident macrophages *in vivo*. Nonetheless, it still presents a pivotal conceptual framework to understand the process and the effect of K21.

Furthermore, the heightened occurrence of TGs was a significant necessity for the inflammatory actions of macrophages, namely in the generation of PGE2. The variations between M1 and M2 fatty acid oxidation, which are more pronounced in M2,[34] may be discussed in detail. Lipid-rich regions exist inside the plasma membrane of mammalian cells and play a crucial role in signal transduction.[35] The presence of these lipid-rich regions induces heightened cellular responses, which are indicative of M2 responses. These responses are dependent on elevated levels of saturated triglycerides, which are necessary for lipid raft-associated receptor-mediated signal transduction.

In this investigation, we examined the impact of K21, a quaternary ammonium silane, on the gene expression profile associated with inflammation in mouse macrophages incited by LPSEc. Our analysis illuminated that LPSEc stimulation precipitated an extensive upregulation of pro-inflammatory markers, notably interleukins (*e.g.,* IL-1α, IL-1β, IL-6, IL-17β, IL-33), CXC chemokines (*e.g.*, Cxcl-1, Cxcl-9, Cxcl-13), chemokine receptors (*e.g.*, Cxcr-1, Cxcr-2, Cxcr-4, Cxcr-5), and components of the complement system (*e.g.,* C1s, C1qa, C2, C4a, C6), delineating a broad activation of inflammatory pathways. However, our findings indicated that K21 treatment markedly reversed this upregulation, attenuating the inflammatory response. This modulation of gene expression by K21 underscores its potential utility in mitigating inflammatory responses, which is pivotal in bacterial infections where excessive inflammation can lead to significant tissue damage.

The noteworthy aspect of K21 mechanism, evident from its downregulation of chemokines and their receptors, suggests a strategic curtailing of immune cell recruitment and activation, which are seminal in orchestrating the inflammatory response. Additionally, the modulation of complement system components by K21 further accentuates its potential in alleviating complement-mediated exacerbation of inflammation, a critical factor in the pathogenesis of various inflammatory diseases. Thus, the comprehensive modulation of the inflammatory milieu by K-21, spanning across cytokines, chemokines, and complement system components, highlights its multifaceted therapeutic potential.

The component of the cytoskeleton of most human gingival fibroblasts is directly concerned to the issue of adhesion and cellular mobility is the actin-based microfilament

system.[36] The results may reflect the effects of ambient variables and laboratory-specific techniques that are difficult to eradicate. These factors can complicate study findings and hinder the ability to apply them to humans. Histological alterations were assessed to determine the quality of wound healing with haematoxylin and eosin and Masson. During the stages of inflammation and proliferation, it is crucial to reduce the intensity of the inflammatory response and increase the expression of repair factors. Efficient management of inflammation helps protect fibroblasts from inflammatory substances, which speeds up the shift of wound healing from the proliferation stage to the remodeling stage[37] with a greater amount of collagen fibres, which were observed in the regenerated K21 exposed specimens when examined at a high magnification using Masson imaging. This indicates that the regenerating tissue exhibited improved effectiveness in mending. This is due to their ability to effectively eliminate germs, promote the deposition of collagen fibres, and reduce inflammation. The successful incorporation of silane within the collagen matrix generates new bonding arrangements in terms of C−Si−O, Si−O−Si and Si −O−C bonding triggering the polycondensation of silanol groups and cross-linking of -OH groups present in collagen fibres.[38]

As with all animal models, it evidently presents some drawbacks that may hinder proper study of the immune response and inflammatory processes. Some biological analysis tools are, for example, lacking, such as antibodies. Certain genes involved in important inflammatory pathways need to be evaluated more, suggesting that some molecular functions are exerted by distantly related, or even unrelated effectors. The development of single-cell -omics approaches have, however, allowed to circumvent some of these disadvantages, making our model to study inflammation in connection to normal physiopathology.[39,40]

Conclusion

In summary, our work demonstrates the effectiveness of K21 antimicrobial in both killing microorganisms and promoting tissue healing and repair, providing evidence for its potential in enhancing the healing process. The material is biocompatible and is presently employed in formulations authorised by the US Food and Drug Administration for disinfecting coronal dental cavities. These formulations include a 2% k21 antimicrobial cavity cleaner, Fitebac, and an aqueous ethanol solution. Further investigation via clinical trials is necessary to determine the effectiveness of this treatment in promoting efficient wound regeneration and healing.

Conflict of interest

None disclosed.

Ethics approval and consent to participate

The project obtained permission from the Institutional Review Board of International Medical University Kuala Lumpur. Obtained written informed consent from all persons who contributed extracted teeth for the laboratory in-vitro experiments approved by the ethics committee.

Consent for publication

Consent for publishing has been obtained from all authors.

Availability of data and materials

All data, code, and resources utilised in the study are accessible to any researcher for the aim of replicating or expanding upon the analysis. The datasets produced and/or examined during the present investigation are not accessible to the public owing to confidentiality concerns. However, interested parties may get them from the corresponding author upon a reasonable request.

Acknowledgements

The authors express gratitude to the laboratories at IMU and Mimos Research Centre for their assistance in conducting research experiments and analysis. The authors would like to express our special thanks to our mentor Professor Frederick Smales for his advice and suggestions and help reading the draft for its grammatical check.

Author Contributions

All authors read and approved the manuscript.

Conceptualisation – Umer Daood, **Data Curation** – Sharjeel Ilyas, Sehar Bashir, Neelofar Yousuf, Maryam Rashid, **Formal Analysis** - Kanwardeep Kaur, Ranjeet Ajit Bapat, Mohammed Nadeem Bijle, Umer Daood, **Funding Acquisition** – Umer Daood, **Investigation** - Muhammad Sharjeel Ilyas, Sehar Bashir, Neelofar Yousuf, Maryam Rashid, Kanwardeep Kaur, Ranjeet Ajit Bapat, Mohammed Nadeem Bijle, **Methodology** - Malikarjuna Rao Pichika, Kit-Kay Mak, Shiming Zhang, Zeeshan Sheikh, Abdul Samad Khan, **Project Administration** – Umer Daood, Ove Peters, Jukka P Matinlinna, Resources, **Software, Supervision** - Ove Peters, Jukka P Matinlinna, **Validation** - Ove Peters, Jukka P Matinlinna, **Visualisation, Writing Original Draft** – Umer Daood, Muhammad Sharjeel Ilyas, **Writing Reviewing and Editing** - Umer Daood, Ove Peters, Jukka P Matinlinna.

Funding

The study protocol was approved by Institutional Research Ethical Committee (538/2021).

Supplementary materials

Supplementary material associated with this article can be found in the online version at doi:10.1016/j.identj.2024.09.012.

REFERENCES

1. Feito M, Casarrubios L, Onaderra M, Gomez-Duro M, Arribas P, Polo-Montalvo A. Response of RAW 264.7 and J774A.1 macrophages to particles and nanoparticles of a mesoporous bioactive glass: a comparative study. Colloids. Surf. B. Biointerfaces. 2021;208:112110.
2. Casarrubios L, Polo-Montalvo A, Serrano MC, Feito MJ, Vallet R, Arcos D. Effects of ipriflavone-loaded mesoporous nanospheres on the differentiation of endothelial progenitor cells and their modulation by macrophages. Nanomater 2021;11:1102.
3. Chen Z, Klein T, Murray RZ, et al. Osteo immunomodulation for the development of advanced bone biomaterials. Mater. Today. 19, 304–321.
4. Tezvergil-Mutluay A, Mutluay M, Gu L, et al. The anti-MMP activity of benzalkonium chloride. J. Dent. 2011;39:57–64.
5. Sica A, Mantovani A. Macrophage plasticity and polarization: in vivo veritas. J. Clin. Investig. 2012;122:787–95.
6. Martinez FO, Gordon S. The M1 and M2 paradigm of macrophage activation: time for reassessment. F1000Prime Rep 2014;6:13.
7. Lindset M, Allenmark S, Thompson RA, Edebo L. Antimicrobial activity of betaine esters, quaternary ammonium amphiphiles which spontaneously hydrolyze into nontoxic components. Antimicro. Agents. Chemo. 1990;10:1949–54.
8. John WM, Jolene YK. Medical implications of antimicrobial coating polymers organosilicon quaternary ammonium chloride. Mod. Chem. Appl. 2013;1:3.
9. Kong K, Kendall C, Stone N, Notingher I. Raman spectroscopy for medical diagnostics—From in-vitro biofluid assays to in-vivo cancer detection. Adv. Drug. Deliv. Rev. 2015;89:121–34.
10. Ong YH, Lim M, Liu Q. Comparison of principal component analysis and biochemical component analysis in Raman spectroscopy for the discrimination of apoptosis and necrosis in K562 leukemia cells. Opt. Express. 2012;20:22158–71.
11. Krafft C, Popp J. The many facets of Raman spectroscopy for biomedical Analysis. Anal. Bioanal. Chem. 2015;407:699–717.
12. Matinlinna JP, Lung CYK, Tsoi JKH. Silane adhesion mechanism in dental applications and surface treatments: a review. Dent. Mater. 2018;34:13–28.
13. Daood U, Matinlinna J, Pichika MR, Kit-Kay M, Fawzy AS. A quaternary ammonium silane antimicrobial triggers bacterial membrane and biofilm destruction. Sci. Rep. 2020;10:10970.
14. Kilkenny C, Browne WJ, Cuthill IC, Emerson M, Altman DG. Improving bioscience research reporting: the ARRIVE guidelines for reporting animal research. Osteoarthr Cartilage 2012;20:25660.
15. International Organization for Standardization. Biological evaluation of medical devices—Part:5 Tests for cytotoxicity (ISO EN 10993-5) and part 12: Sample preparation and reference materials (ISO EN 10993-12). Geneva, Switzerland: International Organization for Standardization; 2009.
16. International Organization for Standardization. Biological evaluation of medical devices—Part:5 tests for cytotoxicity (ISO EN 10993-5) and part 12: Sample preparation and reference materials (ISO EN 10993-12). Geneva, Switzerland: International Organization for Standardization; 2009.
17. Ortega A, Shady F, Ana VO, Nurit B, Juan PR. Antimicrobial evaluation of quaternary ammonium polyethyleneimine nanoparticles against clinical isolates of pathogenic bacteria. IET Nanobiotechnol 2015;9:342–8.
18. Taylor E, Webster TJ. Reducing infections through nanotechnology and nanoparticles. Int. J. Nano med. 2011;6:1463–73.
19. Mosser DM, Edwards JP. Exploring the full spectrum of macrophage activation. Nat. Rev. Immunol. 2008;8:958–69.
20. Heinrich F, Lehmbecker A, Raddatz BB, et al. Morphologic, phenotypic, and transcriptomic characterization of classically and alternatively activated canine blood-derived macrophages in vitro. PloS.ONE 2017;8:e0183572.
21. Meng F, Lowell CA. Lipopolysaccharide (LPS)-induced macrophage activation and signal transduction in the absence of Src-family kinases Hck, Fgr, and Lyn. J. Exp. Med. 1997;185:1661–70.
22. Daood U, Ilyas MS, Ashraf M, et al. Biochemical changes and macrophage polarization of a silane-based endodontic irrigant in an animal model. Sci Rep. 2022;12:6354.
23. Zhang Q, Xiao L, Xiao Y. Porous nanomaterials targeting autophagy in bone regeneration. Pharmaceutics 2021;10:1572.
24. Galvan-Pena S, O'Neill LA. Metabolic reprograming in macrophage polarization. Front. Immunol. 2014;5:420.
25. Daood U, Bapat RA, Sidhu P, et al. Antibacterial and antibiofilm efficacy of k21-E in root canal disinfection. Dent. Mater. 2021;37:1511–28.
26. Notingher I, Bisson I, Bishop AE, et al. In situ spectral monitoring of mRNA translation in embryonic stem cells during differentiation in vitro. Anal. Chem. 2004;76:3185–93.
27. Notingher I, Selvakumaran J, Hench LL. New detection system for toxic agents based on continuous spectroscopic monitoring of living cells. Biosens. Bio. Electron. 2004;20:780–9.
28. Glass CK, Olefsky JM. Inflammation, and lipid signaling in the etiology of insulin resistance. Cell. Metabol. 2012;15:635–45.
29. Venosa A, Smith LC, Murray A, et al. Regulation of macrophage foam cell formation during nitrogen mustard (NM)-Induced pulmonary fibrosis by lung lipids. Toxicol. Sci. 2019;172:344–58.
30. Nguyen NTP, Nguyen LVH, Tran NMP, et al. The effect of oxidation degree and volume ratio of components on properties and applications of in situ cross-linking hydrogels based on chitosan and hyaluronic acid. Mat. Sci. Eng. C. Mater. 2017;103:109670.
31. Chen WT, Zhao SQ, Ita M, et al. An early neutrophil recruitment into the infectious site is critical for bacterial lipoprotein tolerance-afforded protection against microbial sepsis. J. Immunol. 2020;204:408–17.
32. Bleriot C, Chakarov S, Ginhoux F. Determinants of resident tissue macrophage identity and function. Immunity 2020;52:957–70.
33. Daood U, Ilyas MS, Ashraf M, et al. Biochemical changes and macrophage polarization of a silane-based endodontic irrigant in an animal model. Scientific. Reports. 2022;12:6354.
34. Huang SC, Everts B, Ivanova Y, et al. Cell-intrinsic lysosomal lipolysis is essential for alternative activation of macrophages. Nat. Immunol. 2014;15:846–55.
35. Simons K, Ehehalt R. Cholesterol, lipid rafts, and disease. J. Clin. Invest. 2002;110:597e603.
36. Ahangar P, Mills SJ, Smith LE, Gronthos S, Cowin AJ. Human gingival fibroblast secretome accelerates wound healing through anti-inflammatory and pro-angiogenic mechanisms. NPJ Regen Med 2020;10(5):24.
37. Wang W, Gao Y, Xu W, et al. The one-stop integrated nano agent based on photothermal therapy for deep infection healing and inflammation inhibition. Adv. Mater. 2024;36(3):456.
38. Dhand C, Balakrishnan Y, Theng Ong S, et al. Antimicrobial quaternary ammonium organosilane cross-linked nanofibrous collagen scaffolds for tissue engineering. Int J Nanomedicine 2018;13:4473.
39. Choi TY, Choi TI, Lee YR, Choe SK, Kim CH. Zebrafish as an animal model for biomedical research. Exp. Mol. Med. 2021;53:310–7.
40. Buchan KD, van Gent M, Prajsnar TK, et al. Human-Specific Staphylococcal Virulence Factors Enhance Pathogenicity in a Humanised Zebrafish C5a Receptor Model. J. Cell Sci. 2021;134:453–61.